We are IntechOpen, the world's leading publisher of Open Access books Built by scientists, for scientists

4,800
Open access books available

122,000
International authors and editors

135M
Downloads

Our authors are among the

154
Countries delivered to

TOP 1%
most cited scientists

12.2%
Contributors from top 500 universities

CLARIVATE ANALYTICS BOOK CITATION INDEX INDEXED

WEB OF SCIENCE™

Selection of our books indexed in the Book Citation Index in Web of Science™ Core Collection (BKCI)

Interested in publishing with us?
Contact book.department@intechopen.com

Numbers displayed above are based on latest data collected.
For more information visit www.intechopen.com

Chapter 8

Polymer Micro/Nanofibre Waveguides for Optical Sensing Applications

Fuxing Gu, Li Zhang and Heping Zeng

Additional information is available at the end of the chapter

http://dx.doi.org/10.5772/60626

Abstract

This chapter focuses on polymer micro/nanofibre (PMNFs) waveguides and their applications in sensing applications. The PMNFs are functionalized by doping with dyes or blending with solvated polymers before the drawing process. Based on the evanescent wave-coupling technique, the excitation light is efficiently coupled into the PMNFs using silica-fibre tapers and guided along the long-length PMNF waveguides. Due to the tight confinement, the interaction of light with PMNFs is significantly enhanced. Intriguing advantages such as enhanced excitation efficiency, low excitation power operation and high photostability are obtained. On the basis of the optical response when exposed to specimens, functionalized PMNFs are used for humidity, NO_2, and NH_3 detection with high sensitivity and fast response. By using a simple and low-cost nanoimprinting technique, PMNF Bragg gratings are also demonstrated for strain sensing with a high sensitivity of −2.5 pm/με.

Keywords: Polymer, micro/nanofibre, waveguides, sensors, evanescent wave coupling

1. Introduction

In the past few decades, nanotechnology has created a tremendous amount of excitement in various scientific and technological areas, and it is anticipated that it will revolutionize the world in the future. Fundamental to this revolution is the development of novel nanomaterials. Due to size-related effects, nanomaterials exhibit unique property advantages over their bulk forms, including in physical, chemical, optical, electrical, magnetic and other properties, which

can be used to develop novel sensors [1–9]. In contrast to electrical schemes, optical sensing offers potentials of high sensitivity, fast response, immunity to electromagnetic interference, and safe operation in explosive or combustive atmospheres, as well as more options for signal retrieval from optical intensity, spectrum, phase, polarization, and fluorescence lifetime. Nanomaterial-based optical sensors can also be expected to exhibit further advantages, such as higher-integration density and higher efficiency of energy utilization, over conventional sensors.

Recently, polymer micro/nanofibres or nanofibres (PMNFs) have been proven to be promising building blocks for integrating nanoscale optoelectronic devices [10–27]. Compared to those of other glass and semiconductor nanowires and nanofibres, polymers [28] offer a number of highly attractive advantages for sensing applications. First, gas molecules to be detected can be either selectively bound to their surface or diffused into the polymer matrix, which is difficult for other materials such as semiconductors and glasses. Second, polymers can be doped with a wide range of functional dopants, from metal oxides and fluorescent dyes to enzymes that can be used to tailor the properties of the PMNFs with greater versatility, which offers plentiful choices for sensing schemes. Thirdly, operations including doping and drawing are easy to carry out at room temperature, and the doping concentrations are higher than those in glass fibres. Other advantages of polymer materials such as mechanical flexibility, biocompatibility, easy processing and surface modification for the attachment of active compounds [29], and low cost, offer further opportunities for PMNFs over semiconductors and glass fibres in optical sensing applications. Due to these advantages, various sensing devices based on PMNFs have been demonstrated. In this chapter we will focus on the PMNF waveguides, in which the light is coupled based on the evanescent wave-coupling technique, and their optical sensing applications.

2. Optical guiding in PMNFs

Usually the PMNFs used have lengths of around several hundred micrometres and diameters of around several hundred nanometres. Compared with irradiation excitation, which relies on free-space light (Figure 1a), the optical guiding approach in wavelength-scale waveguides can significantly enhance the interaction of light with materials [30–33]. First, the optical guiding configuration that forces light along the length of the PMNF (~100 μm) offers a much larger absorbing length than the thickness of the PMNF (~100 nm) in the irradiation approach. Second, in the irradiation configuration only a small fraction (less than 1%) of irradiated light can be intercepted by the PMNFs, while the evanescent coupling technique with adiabatic fibre taper condensation ensures high coupling efficiency (up to 50%) for transferring light into the PMNFs much more efficiently. Experimental results show that in a 380-nm-diameter 520-μm-length RhB-PS nanofibre, enhanced emission power as high as ~2000 times greater magnitude over the irradiation approach is observed [31]. Theoretical calculation also shows that a visible light with input power of 1 mW is capable of generating a power density of ~1 GW/m^2 inside a 500 nm diameter PMNF. Based on this approach, photodetectors [30,32,33], lasers [34], optical sensors [35–39] and light-emitting nanofibres [31] have been demonstrated in polymer,

semiconductor, and glass micro/nano-waveguides. Compared with the irradiation with micrometre-scale light spot, the optical guiding scheme is best adapted for tightly confined excitation with low cross-talk when multiple PMNFs are closely located – particularly desirable for miniaturization and high-density integration of light-emitting devices.

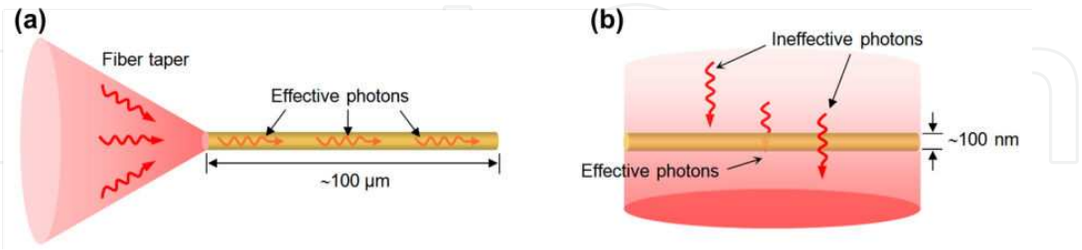

Figure 1. Schematic illustration of the optical guiding (a) and irradiation (b) configurations [30].

3. Fabrication of PMNFs

A number of different techniques, including electrospinning [23], templating [12], mechanical drawing [21,27,36–39], and thermal evaporation methods [40] have been used to fabricate PMNFs. Here we focus on the direct drawing method due to its advantages of simplicity, low cost, and room-temperature operation. As illustrated in Figure 2a, a tungsten probe with a sharp tip (with a diameter of several micrometres) fabricated using an electrochemical etching method was used to transfer a small droplet out of the polymer solution (packed in a quartz cuvette as shown in Figure 2b) onto a glass slide, and then was quickly moved far from to draw a wire out of the droplet. The solvent evaporates instantaneously, leaving a polymer nanofibre on the glass slide (Figure 2c). For example, by using a tungsten probe, polystyrene (PS, *M*w = 100,000; Alfa Aesar) micro/nanofibres are drawn from a chloroform solution containing 5 wt. % PS. Poly-(methyl methacrylate) (PMMA) nanofibres are drawn from an acetone solution containing 5 wt. % PMMA. Polyacrylamide (PAM) nanofibres are drawn from an aqueous solution containing 2 wt. % PAM (*M*w = 5,000,000-6,000,000; Fluka). If a polymer material can be drawn to nanofibres, a blending method can be used to fabricate composite nanofibres. For example, camphorsulphonic acid-doped polyaniline (PANI) nanofibres cannot be drawn from the chloroform solution, but when PS is added into the solution it is easy to draw PANI/PS nanofibres from it. In addition, doped PMNFs can be drawn from a solution that initially dissolves functional dopants such as pH indicators and fluorescent dyes. For example, 250 mg of PS (*M*w = 100 000, Alfa Aesar) and 0.3 mg of rhodamine B (RhB, Alfa Aesar) are dissolved into 2 g of chloroform, and then the mixture is stirred to form a uniform solution.

Using this drawing method, various functionalized PMNFs are obtained with lengths of up to several millimetres with diameters selectable from 100 to several micrometres (Figure 2d), which shows good wave-guiding performance that is easy to handle and has high coupling efficiency at the range of visible and near-infrared wavelength. Figure 3 shows a typical scanning electron microscope (SEM) image of a 310-nm-diameter PS nanofibre doped with

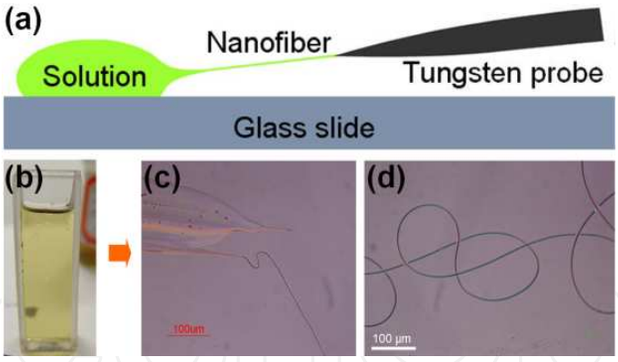

Figure 2. (a) Schematic diagram of the fabrication of the PMNFs. (b) The polymer solution packed in a quartz cuvette. (c) The polymer film and nanofibre after the solvent evaporating. (d) The drawn PMNF [31,38].

RhB, in which the excellent uniformity and sidewall smoothness is clearly seen [31]. For individual PMNFs, the variations of diameter ΔD are very small. For a certain doped PS nanofibre of a diameter of 400 nm, ΔD is about 30 nm over a 1-mm length. The high-resolution SEM image (inset) shows the surface of a doped PS nanofibre clearly and no obvious defect such as porosity is observed.

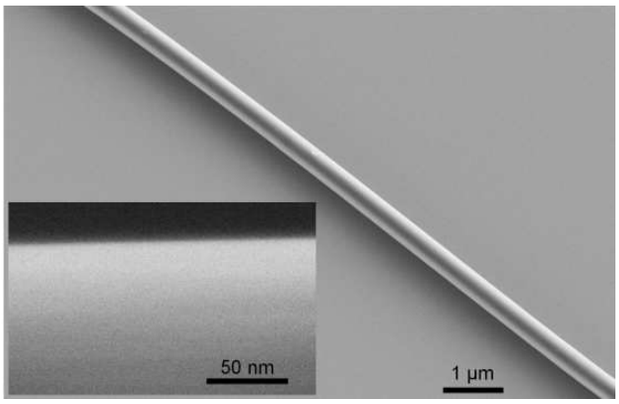

Figure 3. SEM image of a 310-nm-diameter RhB-PS nanofibre. Inset, high-resolution SEM image of the nanofibre [31].

4. Micromanipulation of PMNFs

As-fabricated PMNFs are tailored and manipulated also using tungsten probes (driven by three-axis precision stages) under an optical microscope equipped with super-long-working-distance objectives [31,38,41]. The tungsten probes, with tip sizes of less than 100 nm, can be used to cut PMNFs (Figure 4a). The fibre tapers with sharp tip diameters of less than 300 nm, fabricated from a standard single-mode silica optical fibre (SMF-28e, Corning), can be used to pick up (Figure 1c), transfer, and deposit the PMNFs onto a low-index MgF_2 substrate (refractive index ~1.39), as shown in Figures 4b and 4c.

To obtain a high-stability optical connection and a robust sensing operation, sometimes the PMNFs need to be bonded on a substrate, or their coupling areas with fibre tapers are enclosed

http://dx.doi.org/10.5772/60626

to avoid external interference. For example, in humidity sensing when exposed to high/low RH atmosphere, the PAM nanofibre swells/shrinks slightly due to the diffusion of water molecules, which may change the coupling efficiency between the PAM nanofibre and the fibre taper. The fluoropolymer enclosure can isolate the coupling area from the environment, thus eliminating this effect. For this, the PMNFs or the fibre taper to be enclosed is first placed on the surface of the substrate and positioned using tungsten probes driven by micromanipulators. A micro droplet of a UV-curable fluoropolymer is picked up and cast upon the nanofibre and/or the fibre taper, and is then cured for 10 seconds with a mercury lamp under a nitrogen-gas atmosphere. The refractive index of the cured fluoropolymer is around 1.38 within the visible spectral range, making it suitable for optical isolation of polymer PMNFs with considerably higher indices (e.g., index of the PS is about 1.59). For reference, Figure 4d shows a close-up optical microscope image of a typical coupling area of a 400-nm-diameter PAM nanofibre and a silica-fibre taper (about 550 nm in diameter), which is enclosed by a cured fluoropolymer droplet on a MgF_2 substrate [38].

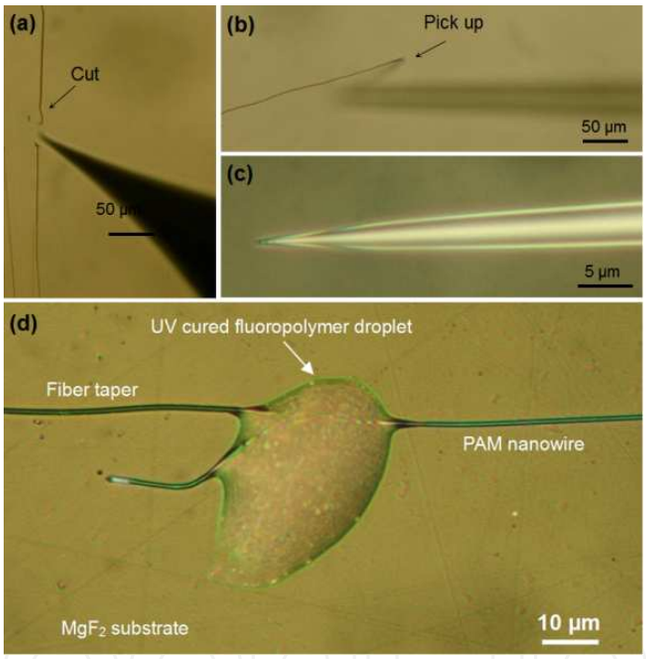

Figure 4. (a) Cutting a nanofibre using a sharp tungsten probe. (b, c) Picking up a nanofibre using a silica-fibre taper with a sharp tip size less than 300 nm. (d) Optical microscope image of a coupling area of a PAM nanofibre and a fibre taper enclosed by a UV-cured fluoropolymer droplet on an MgF_2 substrate [31,38].

5. Light launching and collection

To couple the excitation light efficiently into the PMNFs, we employed the evanescent wave-coupling technique due to its high efficiency and high compactness [31,38,41–44]. In this approach, light is first lens-coupled into a standard silica fibre and then squeezed into a fibre taper with tip diameter ranging from 300 to about 1 μm. The fibre taper is drawn from a

standard optical fibre (SMF-28, Corning) by using a simple flame-heated method. Because the fibre taper is directly connected to the standard optical fibre through the tapering region, the evanescent coupling scheme provides perfect connection between the outer fibre system for processing optical signals and the single micro/nanofibres for optical sensing. As schematically illustrated in Figure 5a, under an optical microscope (Nikon 80i) equipped with super-long-working-distance objectives and using a triple-axis micromanipulator (M-462, Newport), by precisely placing the fibre taper and the PMNF in parallel and close contact within an overlap of a few micrometres, optical near-fields in the fibre taper and the PMNF can strongly overlap, resulting in highly efficient coupling. The close contact between the PMNFs and the fibre tapers can be maintained by van der Waals and electrostatic attraction. The output signals are collected using another fibre taper coupled to the PMNF from the right side as shown.

For active PMNFs, it is convenient to collect outputs such as photoluminescence (PL) using microscope objectives, as illustrated in Figure 5b. The signals are directed to a spectrometer and a CCD camera, respectively. To investigate the polarization behaviours of the emissions, linear polarizers and emission filters are placed between the samples and the detectors.

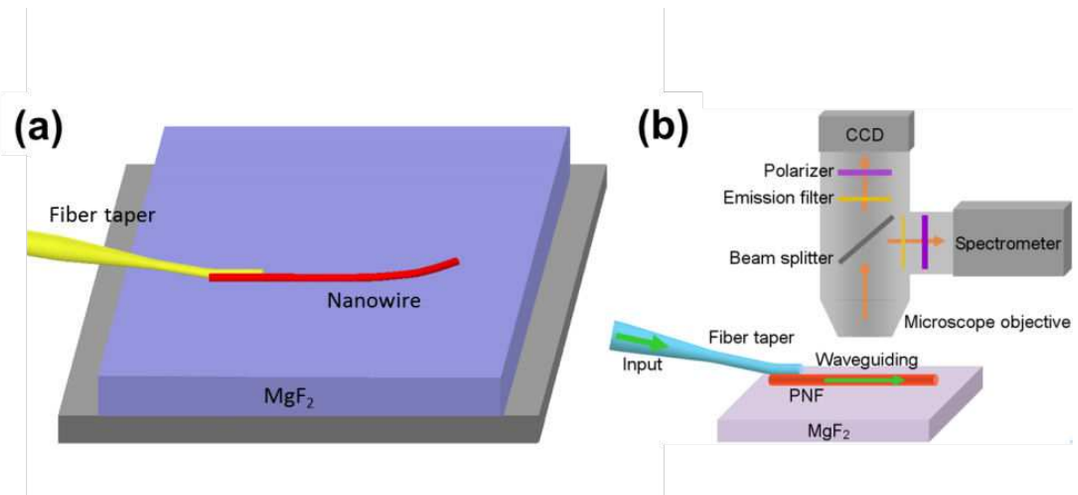

Figure 5. (a) Schematic diagram of light coupling into a nanowire using a fibre taper. The excitation light is launched into the nanofibre based on the evanescent wave technique, which is precisely controlled by a micromanipulator. (b) Schematic diagram of an experimental setup for optical guiding of the single nanofibre supported with a low-index MgF_2 substrate. The output and PL emissions are picked up using a long-working-distance objective. Polarizers and emission filters are placed between the samples and the detectors (the spectrometer and the CCD) [31,38].

6. Optical guiding properties of polymer MNWs

Optical waveguides are the basic elements in optical circuits, so we first investigate the optical guiding properties of PMNFs on the substrate. Figure 6a shows a light from a broadband supercontinuum guided through a 440-nm-diameter PS nanofibre (refractive index ~1.59) supported by an MgF_2 crystal (refractive index~1.39) [38]. It is observed that at the coupling area the broad input light is orange, but at the output end of the nanofibre a green light spot

http://dx.doi.org/10.5772/60626

is observed, indicating an obvious "filtering effect" [38,45,46]: when light is guided along the nanofibre, the light with longer wavelength will leak a larger fraction of evanescent wave into the substrate, inducing higher optical losses compared with light with shorter wavelength. It is important to point out that although this filter is not helpful for low-loss optical guiding, it can be exploited to design wavelength-dependent sensors. When the PMNF is supported on the substrate, a short-pass filter effect is observed. When a 473-nm light is inputted into the nanofibre (Figure 6b), a big light spot is seen at the nanofibre end and only a small spot at the coupling area. A rough estimation shows that the coupling efficiency is as high as over 90%.

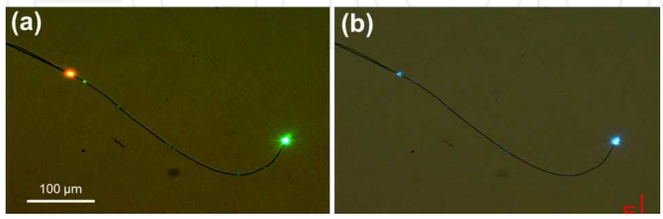

Figure 6. (a, b) Optical microscope image of launching a supercontinuum and 473-nm light into an MgF_2-supported 440-nm-diameter PS nanofibre using a fibre taper, respectively [38].

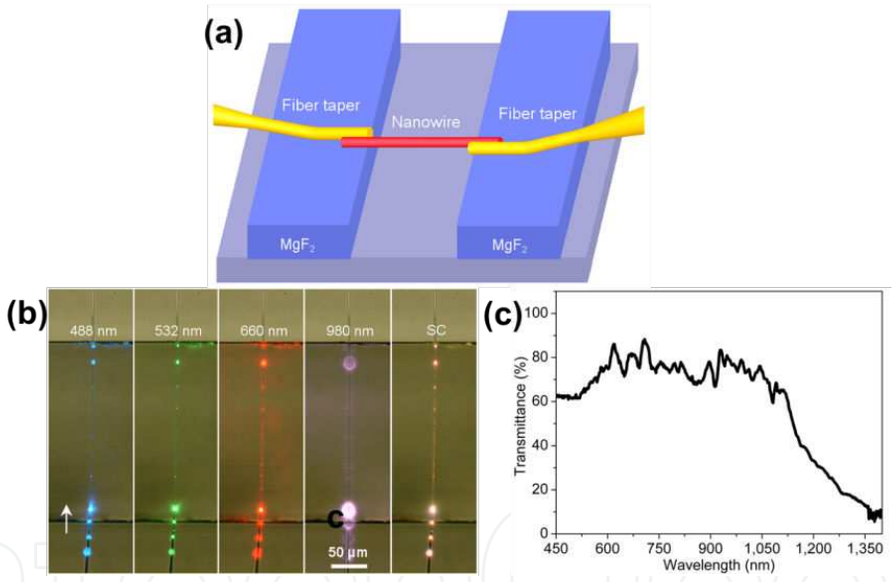

Figure 7. (a) Schematic diagram of a microchannel-supported nanofibre with two ends coupled with fibre tapers. (b) Optical micrographs of the nanofibre guiding a broadband supercontinuum (denoted as SC) and monochromatic lasers with wavelengths of 488, 532, 660, and 980 nm, respectively. Scale bar, 50 μm. (c) Broadband transmission spectrum of a 300-nm-diameter PMMA nanofibre [38].

To enable the PMNFs for broadband optical guiding and eliminate the leakage of guided light, we put the PMNFs across a microchannel, as illustrated in Figure 7a [38]. While the two ends of the nanofibre are supported and coupled with fibre tapers on the surface of the substrate, the main part of the nanofibre is placed on the channel. Figure 7b shows the optical images of a 300-nm-diameter PMMA nanofibre (refractive index ~1.49), guiding a broadband supercontinuum and monochromatic lasers (wavelengths of 488, 532, 660, and 980 nm, respectively). It is observed that there are bright light spots at the end of the nanofibre, indicating broadband

transmittability of the nanofibre. The measured optical loss of the nanofibre is typically lower than 0.1 dB/mm, which can be neglectable due to the small effective length (e.g., less than 300 μm) of the nanofibre used. In addition, the suspension configuration also makes it possible to guide light using PMNFs with much smaller diameters, and this is very helpful to speed up the diffusion of specimens and subsequently the response of the nanofibre [7,10].

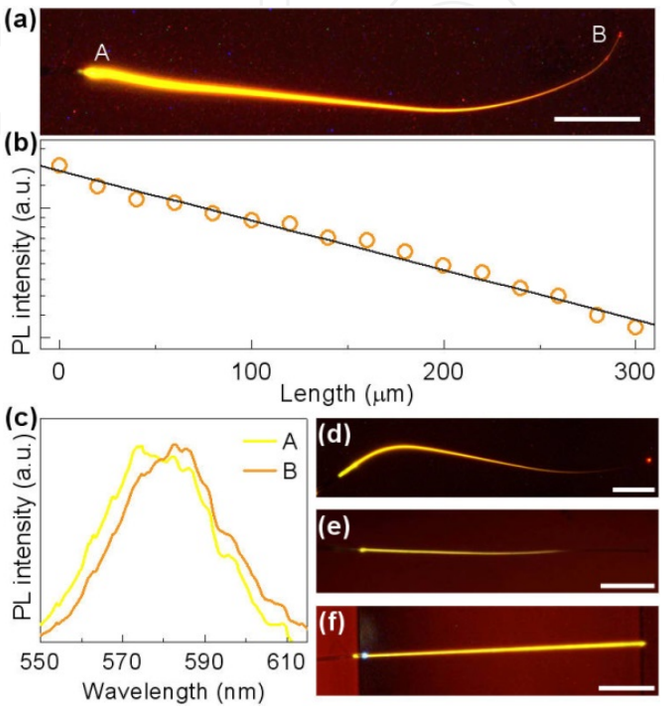

Figure 8. (a) PL optical microscope image of the launching of a 473-nm light into a MgF2-supported 470-nm-diameter RhB-PS nanofibre. (b) PL intensity of the RhB-PS nanofibre as a function of nanofibre length. (c) The comparison of the emission peak at the *A* point and the *B* point. (d) PL optical microscope image of the MgF_2-supported 600-nm-diameter RhB-PS nanofibre. (e) PL optical micrograph of the microchannel-supported 340-nm-diameter nanofibre. (f) PL optical micrograph of the MgF_2-supported 120-nm-diameter nanofibre [31].

Light-emitting sources are also important elements for developing ultra-compactness, so we next investigate the PL of the PMNFs. Figure 8a shows a PL microscope image of a 470-nm-diameter 340-μm-length RhB-PS nanofibre taken with a long-pass emission filter [31]. When a 473-nm laser (λ_{ex}) is launched from the left side with P_{ex} = 100 nW, bright fluorescent emission is generated and guided along the nanofibre. The PL intensity of the RhB-PS nanofibre decreases exponentially with distance along the NF (Figure 8b), attributed to the exponential absorption of the pump light along the nanofibre by fluorescent dyes obeying the Lambert-Beer law [47]. The measured α of the RhB-PS nanofibre at 473 nm is ~50 cm^{-1}. In addition, it is also noticed that the emission peak (λ_{em}) is around 574 nm at the *A* point and 584 nm at the *B* point, as shown in Figure 8c. The redshift of the peak wavelengths is due to the reabsorption of the PL when guided along the nanofibre, and because of the filtering effect the longer wavelengths also suffer relative larger losses, inducing a weak red spot at the *B* point. When we use nanofibres with relative large diameters, a bright red spot is found at the output end of the nanofibre because the PL can be well guided along the nanofibre, as shown in Figure 8d. In contrast, when we use

http://dx.doi.org/10.5772/60626

nanofibres with small diameters, it is found that the PL decays gradually, and no light spot at the output end is observed (Figure 8e) because the excitation light can be well guided along the nanofibre. When using the suspension configuration, the PL can be well excited and guided even using a 120 nm diameter nanofibre, as shown in Figure 8f.

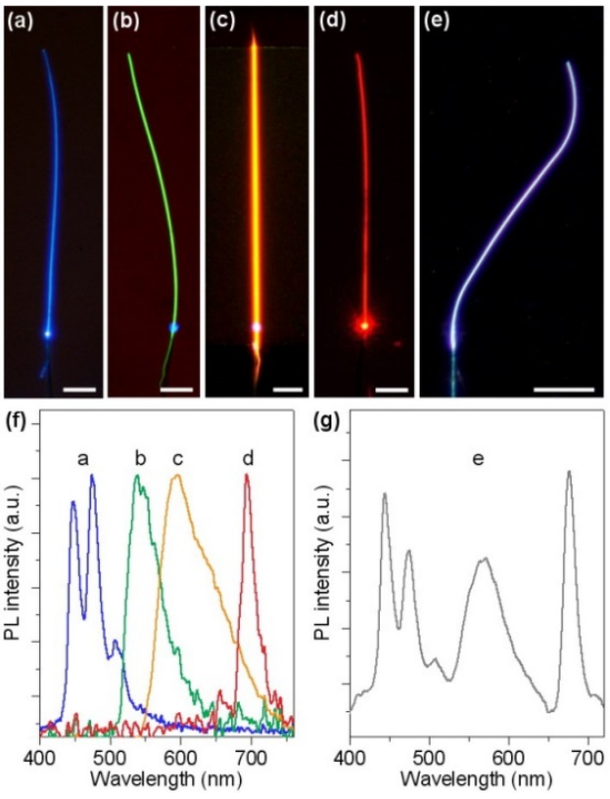

Figure 9. PL microscope images of (a) a perylene-PS nanofibre (380 nm in diameter); (b) a FSS-PAM nanofibre (450 nm in diameter); (c) a Ru(bpy)3Cl2-PAM nanofibre (270 nm in diameter); (d) a ZnPc-PEO nanofibre (610 nm in diameter); and (e) a perylene-RhB-ZnPc-codoped PS nanofibre (430 nm in diameter). In panel (a) λex = 355 nm; in panels (b) and (c) λex = 473 nm; in panel (d) λex = 650 nm and in panel (e) λex = 355 nm. The nanofibres in panels (a), (b), and (d) are supported by MgF2 substrate, and in panel (c) the nanofibre is placed over an MgF2 microchannel. Scale bar: (a–e) 50 μm; (f, g) are PL spectra corresponding to the doped PNFs shown in panels (a–e) [31].

We can also incorporate a variety of fluorescent dyes into PMNFs to generate multicoloured emissions. In Figures 9a to d, we show the optical microscope images of nanofibres doped with four fluorescent dyes [31]: (a) a 360-nm-diameter PS nanofibre doped with perylene, (b) a 450-nm-diameter PAM nanofibre doped with fluorescein sodium salt (FSS), (c) a 270-nm-diameter PAM nanofibre doped with tris(2,2′-bipyridine)ruthenium(II) chloride [$Ru(bpy)_3Cl_2$], and (d) a 610-nm-diameter PS nanofibre doped with zinc phthalocyanine (ZnPc). The FSS-PAM nanofibres are drawn from a water solution containing 0.04 wt. % FSS and 5.5 wt. % PAM. The $Ru(bpy)_3Cl_2$-PAM nanofibres are drawn from a water solution containing 0.07 wt. % $Ru(bpy)_3Cl_2$ and 5.5 wt. % PAM. The ZnPc-PS nanofibres are drawn from a tetrahydrofuran solution containing 0.07 wt. % ZnPc and 5.5 wt. % PS. Their corresponding PL spectra are given in Figure 9f, which covers the whole visible spectral range. Multicoloured or white-light emissions can also be obtained by simultaneously doping two or more fluorescent dyes in a

single nanofibre. Here we show that white-light emission can be generated in perylene-RhB-ZnPc-codoped PS nanofibres drawn from a chloroform solution containing 0.008 wt. % perylene, 0.05 wt. % RhB, 0.22 wt. % ZnPc and 20 wt. % PS. As shown in Figure 9e, when excited by 355-nm light, white-light emission is observed in a perylene-RhB-ZnPc-codoped (430 nm in diameter) PS nanofibre when excited by 355-nm light. The three dyes are distributed homogenously along the whole NF according to the uniform emission in intensity and colour. Figure 9g shows the measured PL spectrum of the perylene-RhB-ZnPc-codoped PS nanofibre, in which the individual peaks agree well with those of the corresponding components in Figure 9f and also covers the whole visible range from 400 to 710 nm.

7. Optical sensing

Next we will introduce two typical PMNF-based sensors: (1) water-soluble polymer-nanofibre humidity sensors, which are based on refractive index changes of the nanofibres [38]; (2) pH-indicator-doped PS-nanofibre ammonia sensors, which are based on absorption changes of the nanofibres [38]. Based on these two underlying mechanisms, many other sensors based on PMNFs have been proposed and demonstrated: by using spectral analysis in the visible/near-infrared region, we introduce selective detection of gas mixtures of NH_3 and humidity [37]. Finally, by using a simple nanoimprinting approach, we introduce the PMNF Bragg gratings and their strain-sensing application [39].

7.1. Methods for gas sensing

Gas detection is particularly important in both environmental protection and human health. Here the gas-sensing experiments are carried out by placing the PMNFs in a sealed glass chamber (see Figure 10a and b) with a gas-flow system and a hygrothermograph for monitoring the relative humidity (RH) [38]. The analyte gas, diluted with air or nitrogen, is introduced while the transmittance of the nanofibre is measured. The mass-flow rate and concentration of the analyte gas are controlled by mass-flow controllers (MFCs). All experiments are carried out at room temperature and atmospheric pressure.

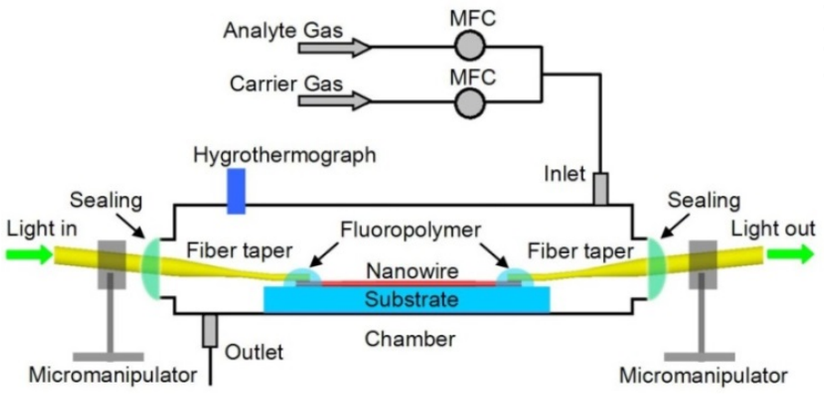

Figure 10. Schematic diagram of sensing experiment [38].

http://dx.doi.org/10.5772/60626

7.2. PMNF sensors based on refractive index changes

We first employ a PAM nanofibre (drawn from a PAM aqueous solution) for relative humidity (RH) sensing. As shown in Figure 11a, a 410-nm-diameter 250-μm-length PAM nanofibre is supported on an MgF_2 substrate, sealed and optically connected to fibre tapers at both ends for evanescent coupling of the probing light. The coupling area is enclosed by a low-index fluoropolymer to isolate it from the disturbing of the water molecules (see inset), because the coupling area is very sensitive to the refractive changes due to the adsorption of water molecules. Figure 11b shows the transmittance of the PAM nanofibre exposed to atmosphere with RH from 35% to 88%, with an average cut-off wavelength of around 545 nm due to the short-pass filter effect. Before the cut-off point, the transmittance decreases monotonously with the increasing RH. The insets show the intensity changes at the wavelength of 532 nm, in which the monotonous dependence can be clearly seen and can be used for RH sensing.

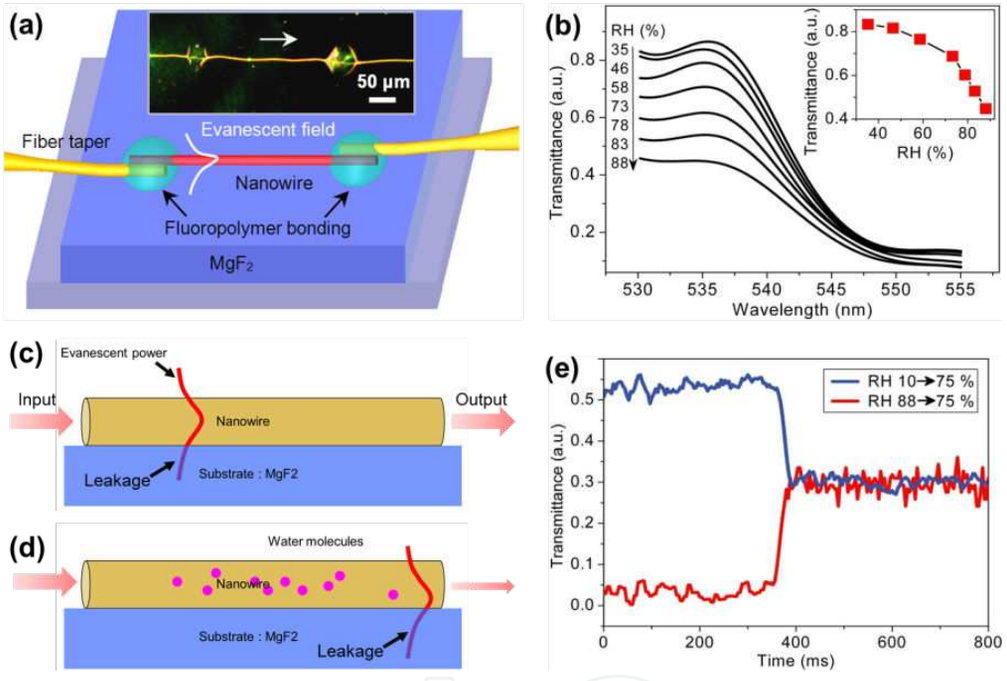

Figure 11. PAM single-nanowire humidity sensors. (a) Schematic illustration of the sensor. Inset, optical microscope image of a 410-nm-diameter PAM nanowire supported on MgF_2 with a 532-nm-wavelength light injected from the left side. The white arrow shows the direction of light propagation. (b) Transmittances of an MgF_2-supported 410-nm-diameter PAM nanowire exposed to an environment of RH from 35% to 88%. Inset, the variation of transmittances at 532 nm wavelength. (c–d) Schematic illustration of the humidity sensor based on evanescent wave leakage. (e) Typical time-dependent transmittance of the sensor reveals the response time of about 24 ms when RH jumps from 10% to 75% and 30 ms when RH falls from 88% to 75% [38].

The underlying mechanism can be explained as follows: when light is guided along the PAM nanofibre, some fraction of the evanescent wave will leak into the substrate [38,43,45,46], as shown in Figure 11c. With the addition of high-RH atmosphere, the refractive index of the PAM nanofibre (about 1.54) decreases due to the diffusion of water molecules, resulting in higher leakage of the guided light nearby and the blue shift of the cut-off wavelength, as shown in Figure 11d. Vice versa, with the addition of low-RH-atmosphere water inside the nanofibre evaporates and the refractive index increases. By alternately cycling 75% and 88%-RH air inside

the chamber the nanofibre exhibits an excellent reversibility. By suddenly changing the humidity in the chamber, the response time of the nanofibre-based humid sensor, with typical time-dependent transmittance shown in Figure 11e. The estimated response time (baseline to 90% signal saturation) of the humid sensor is about 24 ms when RH jumps from 10 to 75%, and 30 ms when RH falls from 88 to 75%. The response time is one or two orders of magnitude shorter than that of existing RH sensors. The remarkably fast response of the humid sensor can be attributed to the small diameter of the nanofibres, which enables rapid diffusion or evaporation of the water molecules as well as fast signal retrieval using the optical approach.

7.3. PMNF sensors based on absorption changes

Doping chemical indicators is another approach to activate the polymer nanofibres for optical sensing. BTB is a pH indicator that has a pH range of 6.0 to 7.6, and can be used to detect basic materials. Here we demonstrate NH_3 gas sensing with a 270-nm-diameter BTB-doped PMMA nanofibre, which is drawn from a chloroform solution containing 0.5 wt. % BTB and 5 wt. % PMMA. The nanofibre is suspended by a 200-μm-width MgF_2 microchannel with a probing light of 660-nm wavelength. As shown in Figure 12a, when nitrogen-diluted NH_3 gas is introduced and diffuses into the nanofibre, the BTB reacts with the NH_3 and changes from acidic form to basic form, resulting in evident absorption of the probing light. Figure 12b shows the optical response of the nanofibre to NH_3 gas cycled with concentrations from 3 to 28 ppm at room temperature, showing linear response (see inset) for NH_3 sensing below 14 ppm with good reversibility. The response time with ammonia at 14 ppm is about 1.8 s, which is much faster than in conventional ammonia sensors.

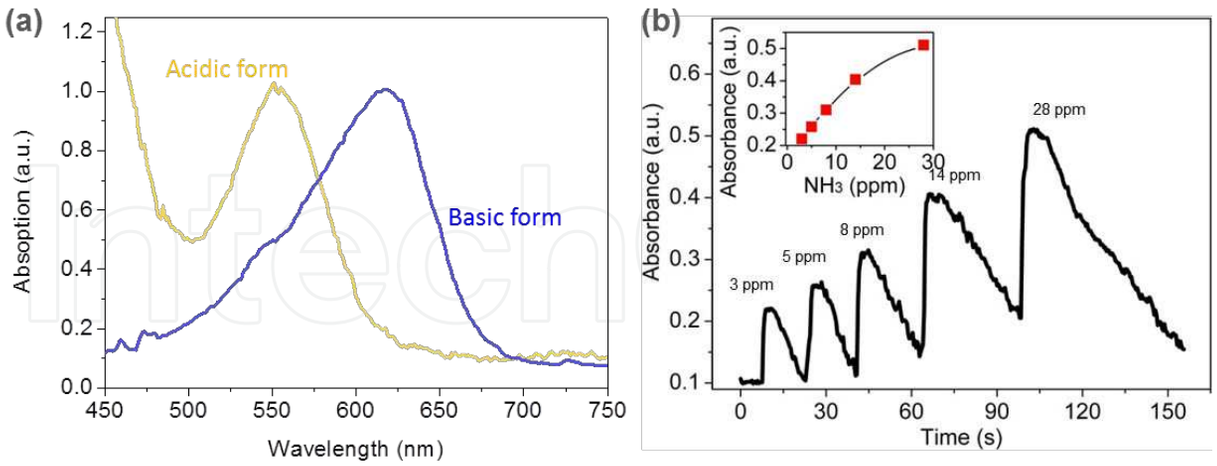

Figure 12. (a) Absorption spectrum of the BTB-doped PMMA nanofibre in acidic form and basic form. (b) Time-dependent absorbance of the nanofibre to NH_3 gas cycled with concentrations from 3 to 28 ppm. Inset, dependence of the absorbance on NH_3 concentration ranging from 3 to 28 ppm [38].

Because of the reversible optical and electrical response to certain gas species, as well as easy processing and environmental stability, doped PANI has been widely used for electrical or

http://dx.doi.org/10.5772/60626

optical detection of a variety of gases such as HCl, NH_3, H_2S and NO_2 [10, 24, 48]. Blending PANI with soluble matrix polymers is essential to fabricate PMNFs, which overcomes its poor mechanical property; the PMNF then shows good mechanical property and low optical loss. Here, PS is used to blend with PANI due to its compatibility with PANI and excellent optical properties, such as good transparency in visible and near-infrared regions and high refractive index (about 1.59). PANI/PS nanofibres are fabricated by direct drawing from polymer-blend solution of 2 wt. % PANI (*M*w = 50 000; Fluka) doped with 10-camphorsulphonic acid (Alfa Aesar) and 5 wt. % PS (*M*w = 100 000; Alfa Aesar) in chloroform.

When exposed to NO_2, the increase of the oxidation degree of PANI results in changes of the spectral absorption, as shown in Figure 13a. Here, a 250-nm-diameter PANI/PS nanofibre is suspended by a 250-μm-width MgF_2 microchannel and optically connected to fibre tapers at both ends. With the addition of 1 ppm NO_2 gas, a clear absorbance at the wavelength of 532 nm is observed in a 250-nm-diameter PANI/PS nanofibre. The response time is about 7 s, which is several orders of magnitude shorter than in other NO_2 sensors. With NO_2 concentration cycled from 0.1 to 4 ppm, the time-dependent absorbance of the nanofibre at room temperature is given in Figure 13b, indicating good reversibility of the nanofibre response.

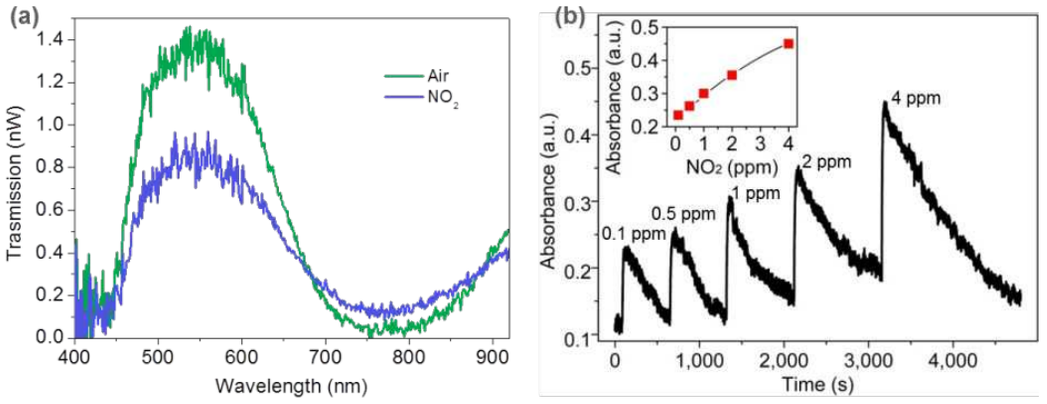

Figure 13. (a) Transmission spectrum of the PANI/PS exposed in air and NO_2 gas, respectively. (b) Time-dependent absorbance of the nanowire to cyclic NO_2/nitrogen exposure with NO_2 concentration from 0.1 to 4 ppm. Inset, dependence of the absorbance over the NO_2 concentration ranging from 0.1 to 4 ppm [38].

7.4. Selective detection of gas mixtures of ammonia and humidity

In electrical sensors relying on the electrical conductance change, it is difficult to determine individual responses in gas mixtures with cross-sensitivity. For example, it is difficult to determine individual responses in gas mixtures of NH_3 and humidity with a single PANI-based nanofibre by electrical detection because both of them have similar signal-change trends [49]; however, the spectral selectivity could provide identity information for an analyte at multiple wavelengths, and optical sensing offers the possibility of selective detection of gas mixtures using a single sensing element. Here we demonstrate that by using spectral analysis, highly selective detection of gas mixtures of NH_3 and humidity can be realized based on PANI/

PS single-nanofibre devices. When exposed to NH_3, camphorsulphonic-acid-doped PANI showing emeraldine salt (ES) form can be transferred to the emeraldine base (EB) form. The ES and EB forms absorb light at different spectral regions, which can be used for optical sensing [50]. For example, Figure 14a shows the output spectra output of a 370-nm-diameter PANI/PS nanofibre in dry air and in 20 ppm-NH_3 dry/dry air, respectively. A decrease in absorption (A_r) with around 600-nm wavelength and an increase in A_r with around 830-nm wavelength are observed (Figure 14b). Because of the opposite response of the nanofibre to NH_3 at these two wavelengths, the differential absorbance can be used to quantify the NH_3 concentrations with enhanced sensitivity. The inset of Figure 14b plots the NH_3-concentration dependence of $\Delta A_{600\text{-}835}$; the monotonous dependence in relation to the NH_3 concentration indicates that the PANI/PS nanofibre could function as an NH_3 optical sensor in dry air.

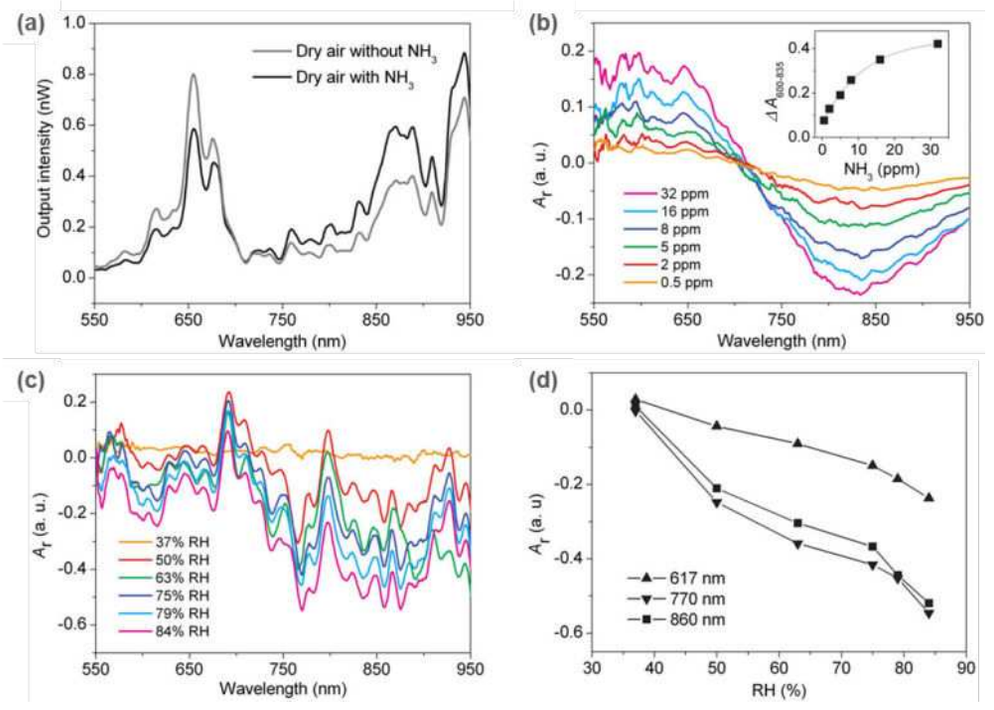

Figure 14. (a) Output intensity of a PANI/PS nanofibre (370 nm in diameter) in dry air without NH_3 (grey line) and with 20 ppm NH_3 (black line). (b) Absorption spectra of the PANI/PS (370 nm in diameter) nanofibre exposed to dry air while the NH_3 concentrations vary from 0.5 to 32 ppm. Inset shows the NH_3-concentration dependence of $\Delta A_{600\text{-}835}$. (c) Absorption spectra of a 350-nm-diameter PANI/PS nanofibre exposed to air with RH ranging from 37% to 84%. (d) RH-concentration dependence of A_r at wavelengths of 617, 770, and 860 nm, respectively [37].

Figure 14c gives the absorption spectra of a 350-nm-diameter PANI/PS nanofibre with RH increasing from 37 to 84%, in which the valleys in the absorption spectra around the wavelengths of 617, 770 and 860 nm decrease with increasing RH level. The changes in the absorption spectra are due to the diffusion of water molecules, which decreases the refractive index of the PANI/PS nanofibre and subsequently changes the coupling efficiency. Figure 14d shows the RH-dependent A_r of the nanofibre with RH ranging from 37 to 84% at the wavelengths of 617, 770 and 860 nm, respectively. The distinct response spectra and underlying mechanism for humidity and NH_3 are apparent and can be used to identify their individual responses using dual-wavelength measurements.

http://dx.doi.org/10.5772/60626

In gas mixtures of NH_3 and humidity, the absorbance of the nanowire at a given wavelength is caused by both NH_3 and RH. Here, 633-nm- and 808-nm-wavelength lights are used to simultaneously monitor the A_r of the 350-nm-diameter PANI/PS nanofibre. Figure 15a shows the time-dependent response of the nanofibre exposed to (1) 84% RH air, (2) 5 ppm NH_3, (3) 5 ppm NH_3 with 79% RH air, and (4) 5 ppm NH_3 with 84% RH air, respectively. The bar graph in Figure 15b summarizes the response of the nanofibre to the analytic gases at 633-nm and 808-nm wavelengths. The height of each bar stands for the maximum A_r of the responses to analytic gases at corresponding wavelengths, in which each analytic gas can be easily distinguished. By solving the simultaneous equations associated with the nanofibre absorptivity, the concentrations of individual gas components can be calculated, along with the sensing length and the fractional energy confined in the nanofibre at each wavelength.

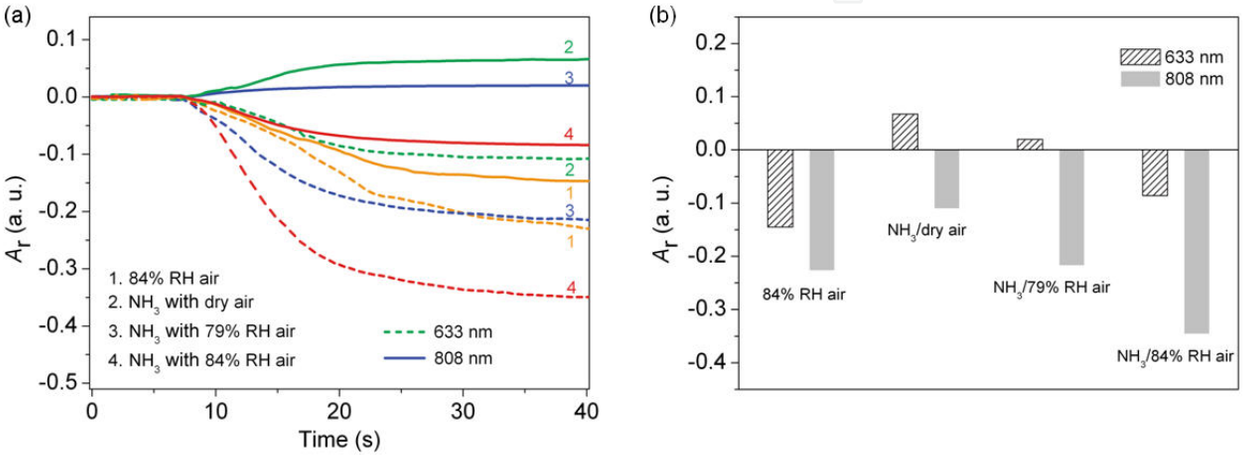

Figure 15. (a) Time-dependent response of the nanofibre exposed to (1) 84% RH air, (2) 5 ppm NH_3, (3) 5 ppm NH_3 with 79% RH air, and (4) 5 ppm NH_3 with 84% RH air, respectively, simultaneously monitored with 633 and 808 nm lasers. (b) Bar graph summarizing the optical response of the nanofibre to the analytic gases at wavelengths of 633 and 808 nm [37].

7.5. PMNF Bragg gratings and their strain-sensing application

Compared with glass material, polymers offer much higher mechanical pliability and smaller Young's modulus E (e.g., 1 GPa for poly(methyl methacrylate) (PMMA) versus 70 GPa for silica glass) [28, 51, 52]. These properties can be exploited to develop optical sensors with higher flexibility and lower force detection limits. Here, benefiting from the easy processing of polymer materials, we report PMNF Bragg gratings by using a simple and low-cost nanoimprinting approach, which consists of three typical steps, as illustrated in Figure 16 [39]. Firstly, PMNFs fabricated by a direct drawing method are placed on a piece of poly(dimethylsiloxane) (PDMS) film for mechanical supporting. Secondly, the PDMS film is heated to a temperature above the glass transition temperature of the PMNF material. A piece of standard-plane reflection grating is used as a mould and a certain pressure is applied onto it. Finally, after the glass substrate has cooled down to room temperature the mould is mechanically removed, with Bragg gratings imprinted on the surface of the MNFs. To optimize the grating effect for guiding modes of the MNF, the grooves of the grating corrugation are kept perpendicular to the MNF axis. In addition, this nanoimprinting approach can be extended to a variety of thermoplastic polymers.

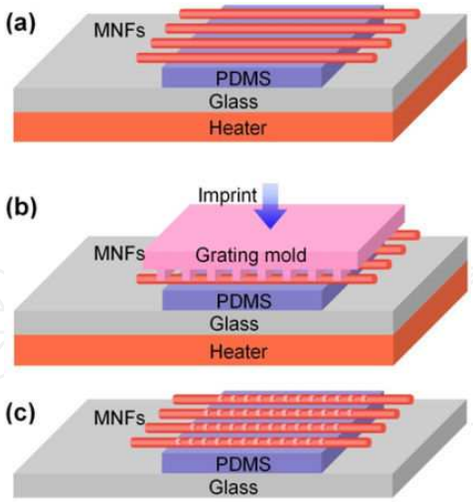

Figure 16. Schematic of the nanoimprinting procedure of PMNF Bragg gratings fabrication, including (a) mechanical supporting, (b) imprinting, and (c) mode removal [39].

Figure 17a shows a scanning electron microscopy (SEM) image of the grating area of an imprinted MNFBG from a 1.3 μm diameter PMMA MNF. It explicitly shows that the grating patterns are uniformly spaced without obvious asymmetric deformation, where the grooves of the grating corrugation are perpendicular to the fibre axis. The grating patterns also show quick gradual transition between the imprinted and un-imprinted regions of the MNF (Figures 17b and c) at the starting parts of the Bragg gratings. Figure 17d reveals an atomic-force-microscopy (AFM) image of a grating segment of 1.2-μm-wide Bragg gratings. Compared with the grating mould (Figure 17e), the Bragg gratings well replicate the 555-nm periodicity of the mould (Figure 17f), with a measured period of about 551 nm and a peak-to-peak depth of about 80 nm. In addition, although the groove depth of the PMNF Bragg gratings is smaller than that of the mould (about 270 nm), the index contrast (Δn ~0.4) between PMMA and the surrounding air is large enough for the waveguide grating demonstrated here.

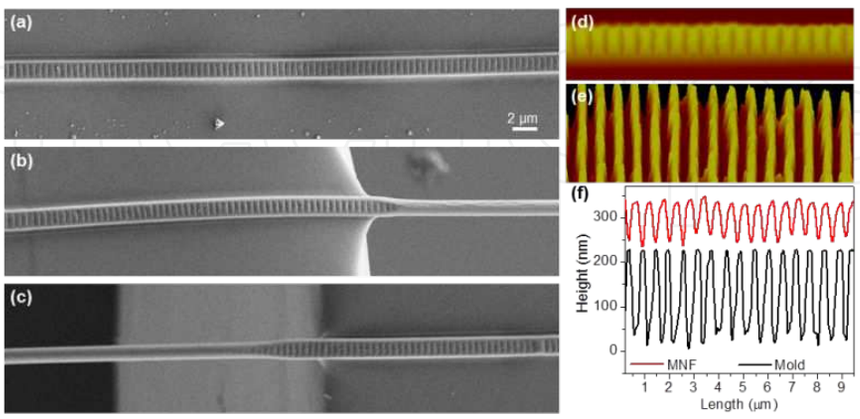

Figure 17. Characterization of PMNF Bragg gratings. (a–c) SEM images of the imprinted PMNF Bragg grating from a 1.3-μm-diameter PMMA PMNF. (d) and (e) AFM images of a grating segment of 1.2-μm-wide PMNF Bragg gratings and the grating mould used, respectively. (f) Groove profiles of the PMNF Bragg gratings and the mould [39].

http://dx.doi.org/10.5772/60626

As-fabricated PMMA PMNF Bragg gratings are placed across an MgF_2 microchannel by micromanipulation, with two ends coupled to silica fibre tapers for optical input and output coupling. Figure 18 shows the transmission and reflection spectra of a PMNF Bragg grating with thickness, width and grating lengths of 1.4, 2.3 and 200 μm, respectively. The two dips centred at 1517 and 1555 nm in the transmission spectrum agree well with the two peaks centred at 1519 and 1554 nm in the reflection spectrum, respectively. Due to the asymmetry of the rectangle-like cross-section and the large refractive index contrast between the MNFBGs and the surrounding air, the guided light with orthogonal polarizations experience high group birefringence, i.e., different modal effective indices (n_{eff}); at the Bragg wavelengths of 1532 and 1510 nm, the calculated quasi-x and quasi-y polarized modes are ~1.39 and ~1.37, respectively, agreeing well with the experimental results at the 1554- and 1519-nm peaks, respectively.

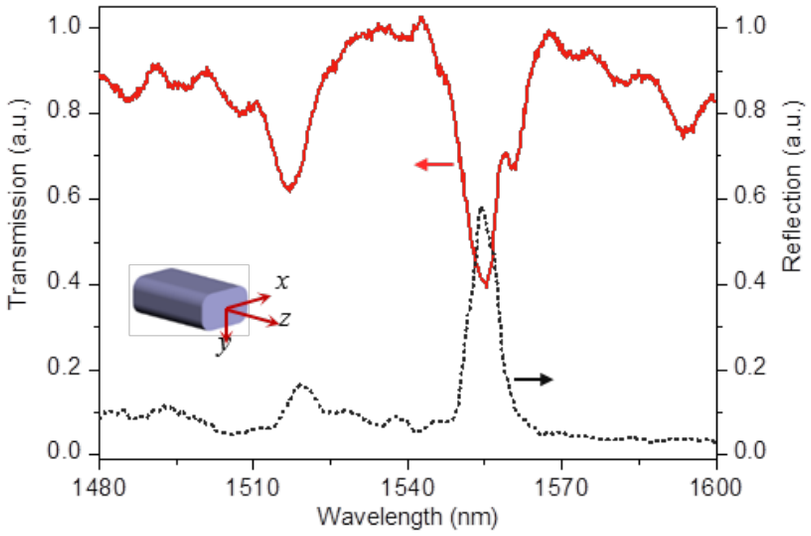

Figure 18. Reflection of PMNF Bragg gratings (2.3-μm wide by 1.4-μm thick) [39].

The strain responses of the PMNF Bragg gratings are investigated. As illustrated in Figure 19a, the PMMA PMNF Bragg grating is placed across an MgF_2 microchannel, and by moving the stage rightwards a tensile force is applied onto it. For robust operation, the coupling area of the fibre taper and the MNF are bonded together by a low-index UV-cured fluoropolymer. Figure 19b shows the transmission spectra changes of an MNFBG (2.5 μm wide by 1.4 μm thick) while the tensile strain increases from 0% to ~4%. The inset shows the Bragg wavelength's (λ) monotonous and linear blueshift from 1590 nm to 1485 nm. The λ shifts of the polymer MNFBG (> 100 nm) are about 10-fold larger compared with those of silica FBGs (usually less than 10 nm). The strain sensitivity ($\Delta\lambda/\lambda$) at 1590 nm is −2.5 pm/με, which is much higher than that of typical silica FBGs (usually ~1.2 pm/με). The blueshift of the λ caused by the tensile strain is different from previous results reported in conventional polymer and silica FBGs, because the grating patterns with a 100-nm depth show a remarkable change in the micro/nanoscale waveguide structures. Upon an axial tensile strain, the MNFBG suffers asymmetric strains and induces large photoelastic effect, which counteracts the elongation-induced redshift effect that is usually dominant in conventional FBGs.

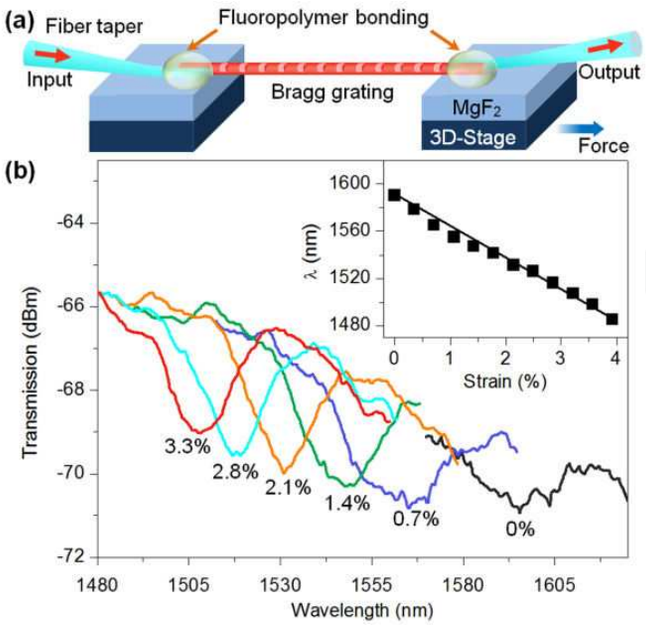

Figure 19. (a) Schematic of experimental setup for strain sensing. (b) Transmission spectra of an MNFBG (2.5 μm wide by 1.4 μm thick) with tensile strain increasing from 0% to ~4%. Top inset: Bragg wavelength shift of the 1590 nm dip under tensile strain from 0% to ~4% [39].

8. Summary

This chapter reviewed PMNF waveguides and their optical sensing applications. The polymer NWs are functionalized by doping with dyes or blending with solvated polymers before the drawing process. Based on the evanescent wave technique using fibre tapers, light is efficiently coupled into PMNFs and guided along the waveguides, with high efficiency and compactness within a broad spectral range. It is shown that in single PMNF waveguides, the tight confinement of light during its propagation along the long length significantly enhances the interaction of light with waveguides by over three orders of magnitude compared with the irradiating approach. Intriguing advantages such as enhanced excitation efficiency, low excitation power operation and high photostability are obtained. On the basis of the optical response when exposed to specimens, functionalized PMNFs are used for humidity, NO_2, and NH_3 detection with high sensitivity and fast response. Selective detection of gas mixture of ammonia and humidity are also realized by using spectral analysis. By using a simple and low-cost nanoimprinting technique, PMNF Bragg gratings are also demonstrated for strain sensing with a high sensitivity of −2.5 pm/με. In addition, the fibre tapers are connected to a standard optical fibre system and this compatibility may stimulate further exploration of PMNFs and PMNFs-based optical sensors for fast and high-sensitive detection in physical, chemical, and biological applications with remote sensing and multiplexing signals in one optical fibre.

http://dx.doi.org/10.5772/60626

Acknowledgements

This work was partly supported by the National Natural Science Foundation of China (11304202 and 91221304), Natural Science Foundation of Shanghai (13ZR1458000), National Key Scientific Instrument Project (2012YQ150092), and National Basic Research Programme of China (2011CB808105).

Author details

Fuxing Gu[1*], Li Zhang[1] and Heping Zeng[1,2,3]

*Address all correspondence to: fuxinggu@gmail.com

1 Shanghai Key Laboratory of Modern Optical System, Engineering Research Centre of Optical Instrument and System (Ministry of Education), School of Optical-Electrical and Computer Engineering, University of Shanghai for Science and Technology, Shanghai, China

2 State Key Laboratory of Precision Spectroscopy, East China Normal University, Shanghai, China

3 Synergetic Innovation Centre of Quantum Information and Quantum Physics, University of Science and Technology of China, Hefei, Anhui, China

References

[1] Xia Y, Yang P, Sun Y, Wu Y, Mayers B, Gates B, Yin Y, Kim F, and Yan H. One-dimensional nanostructures: synthesis, characterization, and applications. Adv Mater. 2003;15(5):353-89.

[2] Stewart ME, Anderton CR, Thompson LB, Maria J, Gray SK, Rogers JA, et al. Nanostructured plasmonic sensors. Chem Rev. 2008;108(2):494-521.

[3] Soci C, ZA, Bao XY, Kim H, Lo Y, and Wang DL. Nanowire photodetectors. J Nanosci Nanotechnol. 2010;10(3):1430-49.

[4] Yan R, Gargas D, Yang P. Nanowire photonics. Nat Photon. 2009;3(10):569-76.

[5] Brambilla G. Optical fibre nanotaper sensors. Opt Fiber Technol. 2010;16:331-42.

[6] Ramgir NS, Yang Y, Zacharias M. Nanowire-Based Sensors. Small. 2010;6(16): 1705-22.

[7] Yang F, KS-C, Cheng M, Hemminger JC, and Penner RM. Smaller is Faster and More Sensitive: The Effect of Wire Size on the Detection of Hydrogen by Single Palladium Nanowires. ACS Nano. 2010;4(9):5233-44.

[8] Li Y, QF, Xiang J, and Lieber CM. Nanowire electronic and optoelectronic devices. Mater Today. 2006;9(10):18-27.

[9] Senesac L, aTTG. Nanosensors for trace explosive detection. Mater Today. 2008;11(3): 28-36.

[10] Liu HQ, KJ, Czaplewski DA, and Craighead HG. Polymeric nanowire chemical sensor. Nano Lett. 2004;4(4):671-5.

[11] Benedetto FD, CA, Pagliara S, Mele E, Persano L, Stabile R, Cingolani R, and Pisignano D. Patterning of light-emitting conjugated polymer nanofibres. Nat Nanotechnol. 2008;3:614-9.

[12] O'Carroll D, LI, and Redmond G. Microcavity effects and optically pumped lasing in single conjugated polymer nanowires. Nat Nanotechnol. 2007;2(3):180-4.

[13] Di Benedetto F, Camposeo A, Pagliara S, Mele E, Persano L, Stabile R, et al. Patterning of light-emitting conjugated polymer nanofibres. Nat Nanotechnol. 2008;3(10): 614-9.

[14] Camposeo A, Di Benedetto F, Stabile R, Neves AA, Cingolani R, Pisignano D. Laser emission from electrospun polymer nanofibers. Small. 2009;5(5):562-6.

[15] Liu H, EJB, Bellan LM, and Craighead HG. Electrospun polymer nanofibers as subwavelength optical waveguides incorporating quantum dots. Small. 2006;2:495-9.

[16] O'Carroll D, LI, and Redmond G. Melt-processed polyfluorene nanowires as active waveguides. Small. 2007;3:1178-83.

[17] Virji S, FJD, Baker CO, Huang JX, Kaner RB, and Weiller BH. Polyaniline nanofiber composites with metal salts: chemical sensors for hydrogen sulfide. Small. 2005;1(6): 624-7.

[18] Vohra V, CG, Destri S, Pasini M, Porzio W, and Botta C. Toward white light emission through efficient two-step energy transfer in hybrid nanofibers. ACS Nano. 2010;4:1409-16.

[19] Kemp NT, MD, Cochrane JW, and Newbury R. Bridging the gap: polymer nanowire device. Adv Mater. 2007;19(18):2634-8.

[20] O'Brien GA, QAJ, Tanner DA, and Redmond G. A single polymer nanowire photodetector. Adv Mater. 2006;18:2379-83.

[21] Ta VD, Chen R, Sun H. Coupled Polymer Microfiber Lasers for Single Mode Operation and Enhanced Refractive Index Sensing. Adv Optical Mater. 2014;2(3):220-5.

[22] Camposeo A, BFD, Stabile R, Cingolani R, and Pisignano D. Electrospun dye-doped polymer nanofibers emitting in the near infrared. Appl Phys Lett. 2007;90:143115.

[23] Huang ZM, ZYZ, Kotaki M, and Ramakrishna S. A review on polymer nanofibers by electrospinning and their applications in nanocomposites. Compos Sci Technol. 2003;63:2223-53.

[24] Huang JX, VS, Weiller BH, and Kaner RB. Polyaniline nanofibers: facile synthesis and chemical sensors. J Am Chem Soc. 2003;125(2):314-5.

[25] Sun H, ZH, Zhang J, Wei H, Ju J, Li M, and Yang B. White-light emission nanofibers obtained from assembling aqueous single-colored CdTe NCs into a PPV precursor and PVA matrix. J Mater Chem. 2009;19:6740-4.

[26] Moran-Mirabal JM, SJD, DeFranco JA, Verbridge SS, Ilic R, Flores-Torres S, Abruna H, Malliaras GG, and Craighead HG. Electrospun light-emitting nanofibers. Nano Lett. 2007;7:458-63.

[27] Xing X, ZH, Wang Y, and Li B. Ultracompact photonic coupling splitters twisted by PTT nanowires. Nano Lett. 2008;8(9):2839-43.

[28] Ma H, JAK-Y, and Dalton LR. Polymer-based optical waveguides: materials, processing, and devices. Adv Mater. 2002;14:1339-65.

[29] Goddard JM, aHJH. Polymer surface modification for the attachment of bioactive compounds. Prog Polym Sci. 2007;32:698-725.

[30] Gu F, ZL, Yu H, Fang W, Bao J, and Tong L. Large defect-induced sub-bandgap photoresponse in semiconductor nanowires via waveguiding excitation. Nanotechnol. 2011;22(42):425201.

[31] Gu F, Yu H, Wang P, Yang Z, Tong L. Light-emitting polymer single nanofibers via waveguiding excitation. ACS Nano. 2010;4(9):5332-8.

[32] Gu F, WP, Yu H, Guo B, and Tong L. Optical quenching of photoconductivity in CdSe single nanowires via waveguiding excitation. Opt Express. 2011;19(11):10880-5.

[33] Gu F, YH, Fang W, and Tong L. Broad spectral response in composition-graded CdSSe single nanowires via waveguiding excitation. Appl Phys Lett. 2011;99(18): 181111.

[34] Yang Q, JX, Guo X, Chen Y, and Tong L. Hybrid structure laser based on semiconductor nanowires and a silica microfiber knot cavity. Appl Phys Lett. 2009;94:101108.

[35] Sirbuly DJ, TA, Law M, Fan R, and Yang P. Multifunctional nanowire evanescent wave optical sensors. Adv Mater. 2007;19:61-6.

[36] Wang P, GF, Zhang L, and Tong L. Polymer microfiber rings for high-sensitivity optical humidity sensing. Appl Opt. 2011;50:G7-G10.

[37] Gu F, YX, Yu H, Wang P, and Tong L. PANI-PS single-nanowire devices for highly selective optical detection of gas mixtures. Opt Express. 2009;17:11230-5.

[38] Gu F, Zhang L, Yin X, Tong L. Polymer single-nanowire optical sensors. Nano Lett. 2008;8(9):2757-61.

[39] Gu F, Yu H, Fang W, Tong L. Nanoimprinted Polymer Micro/Nanofiber Bragg Gratings for High-Sensitivity Strain Sensing. IEEE Photon Technol Lett. 2013;25(1):22-4.

[40] Zhao YS, PA, Fu H, Ma Y, and Yao J. Nanowire waveguides and ultraviolet lasers based on small organic molecules. Adv Mater. 2008;20:1661-5.

[41] Gu F, Zeng H, Zhu Y, Yang Q, Ang L, Zhuang S. Single-Crystal Pd and its Alloy Nanowires for Plasmon Propagation and Highly Sensitive Hydrogen Detection. Adv Optical Mater. 2014;2(2):189-96.

[42] Gu F, Wu G, Zeng H. Hybrid photon–plasmon Mach–Zehnder interferometers for highly sensitive hydrogen sensing. Nanoscale. 2015;7(3):924-9.

[43] Gu F, Zeng H, Tong L, Zhuang S. Metal single-nanowire plasmonic sensors. Opt Lett. 2013;38(11):1826-8.

[44] Gu F, Zhang L, Wu G, Zhu Y, Zeng H. Sub-bandgap transverse frequency conversion in semiconductor nano-waveguides. Nanoscale. 2014;6(21):12371-5.

[45] Chen Y, MZ, Yang Q, and Tong LM. Compact optical short-pass filters based on microfibers. Opt Lett. 2008;33:2565-7

[46] Law M, Sirbuly DJ, Johnson JC, Goldberger J, Saykally RJ, Yang P. Nanoribbon waveguides for subwavelength photonics integration. Science. 2004;305(5688): 1269-73.

[47] Lakowicz JR. Principles of Fluorescence Spectroscopy; 3rd ed. Berlin, Heidelberg: Springer-Verlag; 2006.

[48] Pud A, ON, Korzhenkob A, and Shapovala G. Some aspects of preparation methods and properties of polyaniline blends and composites with organic polymers. Prog Polym Sci. 2003;28(12):1701-53.

[49] Matsuguchi M, OA, and Sakai Y. Effect of humidity on NH_3 gas sensitivity of polyaniline blend films. Sens Actuators B. 2003;94(1):46-52.

[50] Christie S, SE, Persaud K, and Kvasnik F. Remote detection of gaseous ammonia using the near infrared transmission properties of polyaniline. Sens Actuators B Chem. 2003;90:163-9.

[51] Brambilla G, aPDN. The ultimate strength of glass silica nanowires. Nano Lett. 2009;9:831-5.

[52] Peters K. Polymer optical fiber sensors. Smart Mater Struct. 2011;20:013002.